Shared Genomic Regions Underlie Natural Variation in Diverse Toxin Responses

Kathryn S. Evans,*,†,1 Shannon C. Brady,*,†,1 Joshua S. Bloom,‡,§, Robyn E. Tanny,* Daniel E. Cook,*,† Sarah E. Giuliani,* Stephen W. Hippleheuser,* Mostafa Zamanian,†† and Erik C. Andersen*,†,‡‡,2**

*Molecular Biosciences and †Interdisciplinary Biological Sciences Program, Northwestern University, Evanston, Illinois 60208, ‡Department of Human Genetics, §Howard Hughes Medical Institute, and **Department of Biological Chemistry, University of California, Los Angeles, California 90095, ††Department of Pathobiological Sciences, School of Veterinary Medicine, University of Wisconsin, Madison, Wisconsin 53705, and ‡‡Robert H. Lurie Comprehensive Cancer Center, Northwestern University, Chicago, Illinois 60611

ORCID IDs: 0000-0002-1388-8155 (K.S.E.); 0000-0002-3043-1544 (S.C.B.); 0000-0002-7241-1648 (J.S.B.); 0000-0002-0611-3909 (R.E.T.); 0000-0003-3347-562X (D.E.C.); 0000-0001-9233-1760 (M.Z.); 0000-0003-0229-9651 (E.C.A.)

ABSTRACT Phenotypic complexity is caused by the contributions of environmental factors and multiple genetic loci, interacting or acting independently. Studies of yeast and *Arabidopsis* often find that the majority of natural variation across phenotypes is attributable to independent additive quantitative trait loci (QTL). Detected loci in these organisms explain most of the estimated heritable variation. By contrast, many heritable components underlying phenotypic variation in metazoan models remain undetected. Before the relative impacts of additive and interactive variance components on metazoan phenotypic variation can be dissected, high replication and precise phenotypic measurements are required to obtain sufficient statistical power to detect loci contributing to this missing heritability. Here, we used a panel of 296 recombinant inbred advanced intercross lines of *Caenorhabditis elegans* and a high-throughput fitness assay to detect loci underlying responses to 16 different toxins, including heavy metals, chemotherapeutic drugs, pesticides, and neuropharmaceuticals. Using linkage mapping, we identified 82 QTL that underlie variation in responses to these toxins, and predicted the relative contributions of additive loci and genetic interactions across various growth parameters. Additionally, we identified three genomic regions that impact responses to multiple classes of toxins. These QTL hotspots could represent common factors impacting toxin responses. We went further to generate near-isogenic lines and chromosome substitution strains, and then experimentally validated these QTL hotspots, implicating additive and interactive loci that underlie toxin-response variation.

KEYWORDS *C. elegans*; QTL; genetic interactions; toxin; pleiotropy

RAPID advances in sequencing technologies have enabled the collection of high-quality genomic data sets for many species (Mardis 2017). These data, paired with a broad range of high-throughput phenotypic assays, have made quantitative genetics a powerful tool in biology. Linkage mapping has been used to identify quantitative trait loci (QTL), leading to profound impacts on human health (Easton *et al.* 1993; Cowley 2006; Altshuler *et al.* 2008), agriculture and livestock (Rothschild *et al.* 2007; Johnsson *et al.* 2015; Leal-Bertioli *et al.* 2015; Shang *et al.* 2016), and basic biology (Mackay 2001; Andersen *et al.* 2015; Peng *et al.* 2016). Despite the growing number of detected QTL across numerous traits, these QTL often do not explain the complete heritable component of trait variation (Rockman 2012). This missing heritability can be attributed to undetected small-effect additive loci and/or interactions between QTL (Bloom *et al.* 2015). Although some studies contend that epistatic effects among QTL might explain missing heritability (Malmberg *et al.* 2005; Zuk *et al.* 2012; Nelson *et al.* 2013; Lachowiec *et al.* 2015; Mackay 2015), others argue that missing heritability

doi: https://doi.org/10.1534/genetics.118.301311
Manuscript received June 28, 2018; accepted for publication October 16, 2018; published Early Online October 19, 2018.
Available freely online through the author-supported open access option.

Supplemental material available at Figshare: https://doi.org/10.25386/genetics.7158911.
[1]These authors contributed equally to this work.
[2]Corresponding author: Department of Molecular Biosciences, Northwestern University, 3125 Cook Hall, 2205 Tech Drive, Hogan 2-100, Evanston, IL 60208. E-mail: erik.andersen@northwestern.edu

comprises small-effect additive loci that remain undetected in cases where statistical power is too low (Hill *et al.* 2008; Yang *et al.* 2010; Mäki-Tanila and Hill 2014; Ehrenreich 2017). Quantitative geneticists have leveraged large numbers of recombinant strains in both yeast and *Arabidopsis* to overcome power limitations, and concluded that, when power is sufficient, small-effect additive components can be identified that account for nearly all of the heritability of a given trait (Simon *et al.* 2008; Bloom *et al.* 2013, 2015). We require a metazoan system with high statistical power to determine whether this predominantly additive QTL model remains broadly applicable in animals.

One such tractable metazoan is the roundworm nematode *Caenorhabditis elegans*. The genetic variation among a panel of recombinant inbred advanced intercross lines (RIAILs) generated between the N2 and CB4856 strains of *C. elegans* (Rockman and Kruglyak 2009; Andersen *et al.* 2015) has been leveraged in many linkage mapping analyses (Li *et al.* 2006; Gutteling *et al.* 2007a,b; Kammenga *et al.* 2007; Seidel *et al.* 2008, 2011; Doroszuk *et al.* 2009; McGrath *et al.* 2009; Reddy *et al.* 2009; Rockman *et al.* 2010; Viñuela *et al.* 2010; Bendesky and Bargmann 2011; Bendesky *et al.* 2011, 2012; Rodriguez *et al.* 2012; Andersen *et al.* 2014; Glater *et al.* 2014; Snoek *et al.* 2014; Balla *et al.* 2015; Schmid *et al.* 2015; Singh *et al.* 2016; Lee *et al.* 2017; Zdraljevic *et al.* 2017; Zamanian *et al.* 2018). Additionally, a high-throughput phenotyping platform to rapidly and accurately measure animal fitness could provide the replication and precision required to detect small-effect additive loci, and to determine the relative contributions of additive and/or epistatic loci to trait variation (Andersen *et al.* 2014; Zdraljevic *et al.* 2017). Notably, the combination of this panel and phenotyping platform have facilitated linkage mappings of multiple distinct fitness parameters, resulting in the detection of a single QTL, in fact a single quantitative trait gene (QTG), that underlies several fitness-related traits (Andersen *et al.* 2014; Zdraljevic *et al.* 2017). This example of pleiotropy suggests that large-scale studies could reveal additional pleiotropic effects.

Such large-scale studies have implicated pleiotropic QTL that impact the expression of a broad range of genes (Keurentjes *et al.* 2007; Breitling *et al.* 2008; Rockman *et al.* 2010; Hasin-Brumshtein *et al.* 2016). Variation in the master regulators that are within these expression QTL hotspots have downstream effects on the transcription of many genes. Similarly, other QTL hotspots could impact multiple traits, such as responses to various conditions. In yeast, most chemical-response QTL are thought to be unique to one or a few conditions, whereas few QTL have been found to have pleiotropic effects across many conditions (Ehrenreich *et al.* 2012; Knoch *et al.* 2017; Singh *et al.* 2017). Although QTL underlying responses to individual conditions have been identified across multiple animal models (Bubier *et al.* 2014; Marriage *et al.* 2014; Najarro *et al.* 2015; Crusio *et al.* 2016; Highfill *et al.* 2017), the existence of QTL hotspots that influence multiple condition responses has yet to be observed broadly in metazoans.

Here, we performed a set of linkage mapping experiments with a large panel of recombinant lines to identify QTL implicated in responses to 16 different toxins and found three QTL hotspots that underlie many of these responses. We demonstrated how high replication in a high-throughput fitness assay can enable the identification and validation of QTL, even in cases of small phenotypic effects. Additionally, we analyzed relative contributions of additive and epistatic genetic loci in various toxin responses. Finally, we discovered evidence for interactions between loci of the N2 and CB4856 strains that impact several toxin responses, and could suggest how large regions of the genome were swept across the species.

Materials and Methods

Strains

Animals were grown at 20° using OP50 bacteria spotted on modified nematode growth medium, containing 1% agar and 0.7% agarose to prevent animals from burrowing. For each assay, strains were propagated for five generations after starvation to reduce transgenerational effects of starvation (Andersen *et al.* 2014). RIAILs used for linkage mapping were constructed previously (Andersen *et al.* 2015). The construction of near-isogenic lines (NILs) and chromosome substitution strains (CSSs) is detailed below, and all strains are listed in the Supplemental Material. Strains are available upon request.

High-throughput toxin-response assay

We used a modified version of the high-throughput fitness assay described previously (Zdraljevic *et al.* 2017). Populations of each strain were passaged for four generations, amplified, and bleach-synchronized. Approximately 25 embryos from each strain were then aliquoted to 96-well microtiter plates at a final volume of 50 μl of K medium (Boyd *et al.* 2012). Embryos hatched overnight and arrested in the L1 larval stage. The following day, arrested L1 animals were fed HB101 bacterial lysate [Pennsylvania State University Shared Fermentation Facility, State College, PA; (García-González *et al.* 2017)] at a final concentration of 5 mg/ml in K medium and were grown to the L4 larval stage for 48 hr at 20° with constant shaking. Three L4 larvae were then sorted using a large-particle flow cytometer (COPAS BIOSORT; Union Biometrica, Holliston, MA) into microtiter plates that contained HB101 lysate at 10 mg/ml, K medium, 50 μM kanamycin, and either diluent (1% DMSO or 1% water) or diluent and a toxin of interest. The sorted animals were then grown for 96 hr at 20° with constant shaking. During this time, the sorted animals matured to adulthood and laid embryos, yielding a population of parent and progeny in each microtiter well. Prior to the measurement of fitness parameters from the populations, animals were treated with sodium azide (50 mM in M9) to straighten their bodies for more accurate growth-response parameter measurements. Traits that were measured by the BIOSORT

include brood size (n), animal length (time of flight, TOF), and optical density (extinction time, EXT).

Toxin-response trait calculations

Phenotypic measurements collected by the BIOSORT were processed using the R package *easysorter*, which was specifically developed for processing this type of data set (Shimko and Andersen 2014). Briefly, the function *read_data* imported raw phenotypic data then identified and eliminated bubbles. Next, the *remove_contamination* function discarded wells that contained bacterial or fungal contamination (determined by visual inspection) prior to analyzing population parameters. The *sumplate* function then calculated normalized measurements and summary statistics of the assayed traits for the population of animals in each well. The number of animals in each well was divided by the number of animals sorted into that well, yielding a normalized brood size (norm.n). Additionally, optical density (EXT) of each animal was divided by animal length (TOF), resulting in a normalized optical density (norm.EXT) for each animal in each well. The norm.EXT measurement represents the optical density without conflating variation in body length. The summary statistics calculated for each population include the 10th, 25th, 50th, 75th, and 90th quantiles, the mean, and median measurements of TOF, EXT, and norm.EXT, as well as variance for TOF and EXT. Previously, each of these summary statistics has been shown to reveal distinct genetic architectures underlying trait variation, suggesting values to demonstrate the range of biological phenomena that can be captured using this platform (Andersen *et al.* 2015). In total, this analysis resulted in 24 phenotypic measurements for each condition tested. When strains were measured across multiple assay days, the *regress*(*assay = TRUE*) function was used to fit a linear model with the formula (*phenotype* ~ *assay*) to account for differences among assays. Next, outliers were removed by eliminating phenotypic values that were outside two SD of the mean (unless at least 5% of the strains were outside this range in the case of RIAIL assays). Finally, toxin-specific effects were calculated using the *regress*(*assay = FALSE*) function from *easysorter*, which fits a linear model with the formula (*phenotype* ~ *control phenotype*) to generate residual phenotypic values that account for differences between populations that were present in control conditions. For this reason, strain phenotypes in control conditions can influence regressed toxin effects and trait categorizations (below).

Dose-response assays

For each toxin, a dose-response experiment was performed using quadruplicates of four genetically diverged strains (N2, CB4856, DL238, and JU258). Animals were assayed using the high-throughput fitness assay and toxin-response trait calculations were performed as described above (Supplemental Material, File S1). The concentration of each toxin that provided a highly reproducible toxin-specific effect with variation between N2 and CB4856 across three distinct traits (brood size, norm.n; mean length, mean.TOF; and mean optical density, mean.norm.EXT) was selected for linkage mapping experiments. The chosen concentrations and diluents of each toxin are as follows: cadmium 100 μM in water, carmustine 250 μM in DMSO, chlorothalonil 250 μM in DMSO, chlorpyrifos 1 μM in DMSO, cisplatin 250 μM in water, copper 250 μM in water, diquat 250 μM in water, fluoxetine 250 μM in DMSO, Floxuridine (FUdR) 50 μM in water, irinotecan 125 μM in DMSO, mechlorethamine 200 μM in DMSO, paraquat 500 μM in water (50 μM was used for the CSS and NIL assays), silver 150 μM in water, topotecan 400 μM in water, tunicamycin 10 μM in DMSO, and vincristine 80 μM in water (Table S1). The concentration of paraquat differs to the concentration used previously (Andersen *et al.* 2015), suggesting why the genetic architectures are different between the two studies. Toxins assayed in this manuscript were purchased from Fluka Chemical (Buchs, Switzerland) (chlorothalonil, #36791-250MG; chlorpyrifos, #45395-250MG; and diquat dibromide monohydrate, #45422-250MG-R), Sigma ([sigma Chemical], St. Louis, MO) (vincristine sulfate salt, #V8879-25MG; cisplatin, #479306-1G; silver nitrate, #209139; carmustine, #1096724-75MG; and topotecan hydrochloride, #1672257-350MG), Calbiochem (San Diego, CA) (tunicamycin, #654380), Aldrich Chemical (Milwaukee, WI) (mechlorethamine hydrochloride, #122564-5G and cadmium chloride #01906BX), Alfa Aesar (irinotecan hydrochloride trihydrate, #AAJ62370-MD), Bioworld (5-fluoro-2'-deoxyuridine, #50256011), Enzo Life Sciences (fluoxetine, #89160-860), Mallinckrodt (cupric sulfate, #4844KBCK), and Chem Service (paraquat, #ps-366).

Linkage mapping

A total of 296 RIAILs were assayed in the high-throughput fitness assay in the presence of each of the 16 toxins listed above as well as control conditions (water or DMSO, File S2). Linkage mapping was performed on each of the 384 toxin-response traits (16 toxins × 24 population parameters per toxin) using the R package *linkagemapping* (www.github.com/AndersenLab/linkagemapping, File S3). The genotypic data (WS245) and residual phenotypic data were merged using the *merge_pheno* function. QTL were detected using the *fsearch* function, which scaled phenotypes to have a mean of zero and variance of one, then calculated logarithm of odds (LOD) scores for each marker and each trait as $-n(ln(1-R2)/2ln(10))$, where r is the Pearson correlation coefficient between RIAIL genotypes at the marker and trait values (Bloom *et al.* 2013). We noted that this scaling of the data did not impact mappings because scaled and unscaled mappings were identical. The phenotypic values of each RIAIL were then permuted randomly while maintaining correlation structure among phenotypes 1000 times to calculate a significance threshold based on a genome-wide error rate of 5%. The marker with the highest LOD score was then set as a cofactor and mapping repeated iteratively until no significant QTL were detected. Finally, the *annotate_lods* function was used to calculate the fraction of variation in RIAIL phenotypes explained by each QTL. The 95% C.I.s were defined

by markers within a 1.5-LOD drop from the marker with the maximum LOD score.

Principal component analysis of RIAILs

Because some of the 24 population parameters measured by the BIOSORT are highly correlated, a principal component analysis (PCA) was performed. For each growth-response trait, RIAIL phenotypic measurements were scaled to have a mean of zero and a SD of one. The *princomp* function within the *stats* package in R (R Core Team 2017) was used to run a PCA for each toxin. For each toxin, the minimum number of principal components (PCs) that explained at least 90% of the total phenotypic variance in the RIAILs was mapped through linkage mapping (File S4 and Table S2), totaling 97 PCs across all toxins (File S5). We additionally performed a two-dimensional genome scan using the function *scantwo()* in the *qtl* package (Broman *et al.* 2003) for all 47 significantly mapped PCs (File S6). Significant interactions were determined by permuting the phenotype data for each PC 1000 times and determining the 5% genome-wide error rate.

Heritability estimates

Broad-sense heritability was estimated for each of the 97 PCs using the formula $H^2 = (\sigma_R^2 - \sigma_P^2)/\sigma_R^2$, where σ_R^2 and σ_P^2 are the variance among the RIAIL and parental (N2 and CB4856) phenotypic values, respectively (Brem and Kruglyak 2005). A variance component model using the R package *regress* was used to estimate the fraction of phenotypic variation explained by additive genetic factors ("narrow-sense" heritability) (Clifford and McCullagh 2006, 2014; Bloom *et al.* 2015). The additive relatedness matrix was calculated as the correlation of marker genotypes between each pair of strains. In addition, a two-component variance component model was calculated with both an additive and pairwise interaction effect (File S7). The pairwise interaction relatedness matrix was calculated as the Hadamard product of the additive relatedness matrix.

Calculation of hotspots

We estimated centimorgan distances from recombination events in the RIAIL panel to account for nonuniform distribution of genetic diversity across the genome. The genome was divided into 65 total bins with each bin containing 26 cM. To determine if the 82 QTL significantly clustered around particular genomic regions, we set a threshold for significant QTL hotspots based on the 99th percentile of a Poisson distribution with a mean of 1.2 QTL (total QTL/total bins).

Generation of NILs

NILs were generated by crossing selected RIAILs to each parental genotype. For each NIL, eight crosses were performed followed by six generations of propagating isogenic lines to ensure homozygosity of the genome. For each cross, PCR amplicons for insertion–deletion (indel) variants on the left and right of the introgressed region were used to confirm progeny genotypes, and select nonrecombinants within the introgressed region. NILs were whole-genome sequenced as described below to confirm their genotype (File S8). Reagents used to generate NILs and a summary of each introgressed region are detailed in the Supplemental Material. A statistical power calculation was used to determine the minimal number of technical replicates required to observe the predicted phenotypic effect of each QTL at 80% power. These calculations are listed in Table S3. The number of technical replicates tested per assay for any given toxin did not exceed 100 because of experimental timing constraints. The PCs that mapped to each NIL region are those with a QTL with a confidence interval that overlaps with or spans the entire introgressed region in the NILs (Table S4 and Table 1).

Whole-genome sequence library preparation and analysis

DNA was isolated from 100 to 300 μl of packed animals using QIAGEN's Blood and Tissue kit (Valencia, CA; catalog # 69506). Following the ATL lysis step, 4 μl of 100 mg/ml RNAse was added to each sample and allowed to incubate for 2 min at room temperature. DNA concentration was determined using the Qubit dsDNA BR Assay Kit (catalog # Q32850). For each strain, a total of 0.75 ng of DNA was combined with 2.5 μl transposome (kit # FC-121-1011; Illumina) diluted 35× with 1× Tris Buffer (10× Tris Buffer: 100 mM Tris-HCl pH 8.0 and 50 mM $MgCl_2$) in a 10 μl final volume on ice. This reaction was incubated at 55° for 10 min. The amplification reaction for each strain contained (final concentrations): 1× ExTaq Buffer, 0.2 mM dNTPs, 1 U ExTaq (catalog # RR001A; Takara), 0.2 μM primer 1, 0.2 μM primer 2, and 5 μl of tagmentation material from the previous step in a 25 μl total volume. Each strain had a unique pair of indexed primers. We first made a master mix containing buffer, water, dNTPs, and ExTaq, then aliquoted the appropriate volume of this mix into each well. We added the specific primer sets to each well and finally the tagmentation reaction. The amplification reaction was incubated in a thermocycler with the following conditions: 72° for 3 min (1×); 95° for 30 sec (1×); 95° for 10 sec, 62° for 30 sec, and 72° for 3 min (20×); and 10° on hold. We combined 8 μl from each amplification reaction to generate a pool of libraries. A portion of the libraries was electrophoresed on a 2% agarose gel. DNA was excised and gel purified using QIAGEN's Gel Purification Kit (catalog # 28706). The libraries were sequenced on the Illumina HiSeq 2500 platform using a paired-end 100-bp reaction lane. Alignment, variant calling, and filtering were performed as described previously (Cook *et al.* 2016). NIL and CSS genotypes were called using the VCF file and a Hidden Markov Model as described previously (Cook and Andersen 2017).

Generation of chromosome substitution strains (CSS)

CSSs were generated by crossing N2 and CB4856 parental strains, and mating cross progeny, to each parental genotype. For each CSS, eight crosses were performed followed by six generations of propagating isogenic lines to ensure

Table 1 Toxins and PCs mapped per hotspot

Toxin	Class	PCs in IVL	PCs in IVR	PCs in V
Cadmium	Heavy metal	0	0	0
Carmustine[a]	Chemotherapeutic	1[a]	0	1[a]
Chlorothalonil[a]	Pesticide	2[a]	1[a]	1[a]
Chlorpyrifos	Pesticide	1	1	0
Cisplatin[a]	Chemotherapeutic	2[a]	1	2[a]
Copper	Heavy metal	2	0	0
Diquat	Pesticide	0	0	0
Fluoxetine[a]	Neuropharmaceutical	1	2[a]	0
FUdR	Chemotherapeutic	1	1	0
Irinotecan[a]	Chemotherapeutic	0	1[a]	2
Mechlorethamine	Chemotherapeutic	0	0	1
Paraquat[a]	Pesticide	0	0	1[a]
Silver[a]	Heavy metal	3[a]	0	1[a]
Topotecan	Chemotherapeutic	1	0	0
Tunicamycin	Chemotherapeutic	2[a]	0	0
Vincristine	Chemotherapeutic	2	1	0

PC, principal component; IVL, hotspot on the center of chromosome IV; IVR, hotspot on the center of chromosome IV; V, hotspot on the center of chromosome V FUdR, Floxuridine.

[a] Denotes a toxin tested with near-isogenic line and/or chromosome substitution strain assays.

homozygosity of the genome. For each cross, PCR amplicons for indels on the left and right of the introgressed region were used to confirm progeny genotypes and select nonrecombinants within the introgressed region. CSSs were whole-genome sequenced as described above to confirm their genotype (File S8). Reagents used to generate CSSs are detailed in the Supplemental Material. As described for NIL assays, power calculations were performed to determine the number of technical replicates required to observe the predicted phenotypic effect of the CSSs.

Selection of traits to categorize in CSS and NIL assays

Pairwise correlations of RIAIL phenotypes among the 24 growth-response traits measured by the BIOSORT were calculated using the *cor* function within the *stats* package in R, with the *use* argument set to "pairwise.complete.obs." For each toxin, hierarchical clustering was performed using the function *hclust* from the *stats* package (R Core Team 2017). *Cutree* was then used to group the resulting dendrogram into k groups, where k is equal to the minimum number of PCs that explained at least 90% of the phenotypic variance in the RIAILs. For each PC that mapped to a hotspot, the growth-response trait that was most correlated to that PC, as well as all growth-response traits within that cluster of the dendrogram, were assayed in NIL and CSS experiments (File S9 and Table 2).

Categorization of CSS and NIL results

Toxin responses for NILs and CSSs were tested using the high-throughput fitness assay for traits correlated with mapped PCs as described above (File S10 and Table 2). Complete pairwise statistical analyses of strains was performed for each trait tested in all CSS and NIL assays (Tukey's honest significant difference test, File S11). A P-value of $P < 0.05$ was used as a threshold for statistical significance. NIL recapitulation was defined by the significance and direction of effect of the NIL compared to the parental strains. Six categories were defined: (1) "no parental difference," (2) "recapitulation," (3) "no QTL effect," (4) "bidirectional interaction," (5) "unidirectional interaction," and (6) "miscellaneous" (Table 3). Traits for which N2 and CB4856 phenotypes were not statistically different comprise the "no parental difference" category and were not further categorized. Traits in the "recapitulation" category must satisfy the following criteria: significant difference between the parental strain phenotypes, significant difference between phenotypes of each NIL and the parent that shares its background genotype, and both NILs must display the expected direction of effect of the introgressed genotype. Traits with "no QTL effect" displayed a significant parental phenotypic difference and the phenotype of each NIL was not statistically different from the phenotype of the parent sharing its background genotype. Traits that have a "bidirectional interaction" must display a significant parental phenotypic difference, the phenotypes of both NILs must be significantly different from phenotypes of both parents, and the phenotypes of both NILs must be transgressive (lie beyond the phenotypic range of the parental strains). Lastly, traits with a "unidirectional interaction" were categorized similarly to the bidirectional interaction, except only one NIL must display a transgressive phenotype, and the other NIL either shows no QTL effect or recapitulation. Traits that did not fit these descriptions were categorized as "miscellaneous".

Traits in the chromosome V hotspot were further categorized using the combined data from both the CSS and NIL assays. Seven categories were defined: (1) "no parental difference", (2) "recapitulation", (3) "no QTL effect", (4) "external interchromosomal interaction" (uni- or bidirectional), (5) "internal interchromosomal interaction" (uni- or bidirectional), (6) "intrachromosomal interaction" (uni- or bidirectional), and (7) "miscellaneous" (Table 4). No parental difference was defined by traits in which the parental strains were either not significantly different from each other or did not have the same direction of effect in both the CSS and NIL assays. "Recapitulation" and "no QTL effect" traits were defined by traits that were classified as either recapitulating or no QTL effect, respectively, in both assays. Traits displaying an "external interchromosomal interaction" show evidence for interaction in the CSS but no interaction (either recapitulating or no QTL effect) in the NIL. On the other hand, traits displaying an "internal interchromosomal interaction" showed evidence of the same interaction for both the CSS and the NIL assays. Finally, traits displaying an "intrachromosomal interaction" showed evidence of an interaction in the NIL but not in the CSS assay. All other traits that did not fit these descriptions were categorized as "miscellaneous" (File S12).

Statistical analysis

All statistical tests of phenotypic differences in the NIL and CSS assays were performed in R (version 3.3.1) using the

Table 2 All traits tested in NIL and CSS assays

PC	Hotspot	Correlated traits	Correlation range
Carmustine.PC1	V	mean.EXT, mean.TOF, q75.EXT, median.EXT, median.TOF, q75.TOF, median.norm.EXT, q90.TOF, q90.EXT	0.72–0.95
Carmustine.PC6	IVL	q25.norm.EXT, q10.norm.EXT	0.33–0.39
Chlorothalonil.PC1	V	mean.EXT, q75.EXT, mean.TOF, median.EXT, median.TOF, q75.TOF	0.73–0.95
Chlorothalonil.PC2	IVL	cv.TOF, cv.EXT	0.72–0.90
Chlorothalonil.PC3	IVL, IVR	mean.norm.EXT, q75.norm.EXT, q90.norm.EXT, median.norm.EXT	0.50–0.65
Cisplatin.PC1	IVL, V	mean.EXT, mean.TOF, median.EXT, median.TOF, q75.TOF, q75.EXT, q90.EXT, q90.TOF	0.78–0.97
Cisplatin.PC3	IVL	var.TOF, var.EXT	0.38–0.54
Cisplatin.PC4	V	norm.n, n	0.76–0.80
Fluoxetine.PC1	IVR	mean.norm.EXT, q75.norm.EXT, mean.EXT, q75.EXT, q90.norm.EXT, q90.EXT	0.79–0.96
Fluoxetine.PC5	IVR	q90.norm.EXT, q75.norm.EXT, mean.norm.EXT, q75.EXT, mean.EXT, q90.EXT	0.07–0.40
Irinotecan.PC2	IVR	cv.TOF, cv.EXT	0.57–0.84
Paraquat.PC1	V	median.EXT, mean.EXT, q25.EXT, q75.EXT, mean.TOF, q75.TOF, q10.EXT, q90.EXT, q90.TOF, median.TOF, q25.TOF, q10.TOF	0.75–0.95
Silver.PC1	V	mean.EXT, median.EXT, q75.EXT, mean.TOF, q90.EXT, q90.TOF, median.TOF, q75.TOF	0.77–0.96
Silver.PC3	IVL	q10.norm.EXT, q25.norm.EXT, mean.norm.EXT, median.norm.EXT, q75.norm.EXT, q90.norm.EXT	0.32–0.64
Silver.PC4	IVL	n, norm.n	0.84–0.84
Silver.PC5	IVL	n, norm.n	0.41–0.41
Tunicamycin.PC1	IVL	median.EXT, q75.EXT, mean.TOF, q75.TOF, median.TOF, median.norm.EXT, q90.EXT, q90.TOF, mean.EXT, q75.norm.EXT, mean.norm.EXT, q25.norm.EXT, q90.norm.EXT, q10.norm.EXT	0.69–0.96
Tunicamycin.PC3	IVL	norm.n, n	0.47–0.50

PC, principal component; V, hotspot on the center of chromosome V; EXT, extinction; TOF, time of flight; IVL, hotspot on the center of chromosome IV; IVR, hotspot on the right of chromosome IV.

TukeyHSD function (R Core Team 2017) on an ANOVA model with the formula (*phenotype* $\sim$ *strain*). The *P*-values of individual pairwise strain comparisons were reported and a *P*-value of $P < 0.05$ was deemed significant. The direction of effect of each NIL was determined by comparing the median phenotypic value of the NIL replicates to that of each parental strain. NILs whose phenotypes were significantly different from both parents and whose median lied outside of the range of the parental phenotype medians were considered hypersensitive or hyperresistant. Comparing LOD scores, and variance explained between traits with "no parental effect" and traits with a significant parental effect in the NIL assays, was performed using a Wilcoxon rank sum test with continuity correction using the *wilcox.test* function in R (R Core Team 2017).

Data availability

File S1 contains results of the dose response assays for all toxins. File S2 contains the residual phenotypic values for each RIAIL for each trait. File S3 contains the linkage mapping results for the 384 toxin-response traits tested with the high-throughput assay (HTA). File S4 contains the phenotypic values for each RIAIL for each of the significant PCs. File S5 contains the annotated QTL and confidence intervals identified through linkage mapping for PCs. File S6 contains the results of a two-factor genome scan for all PCs with a significant QTL identified with linkage mapping. File S7 contains the broad-sense heritability estimates, as well as additive and interactive components of heritability for each PC. File S8 is a VCF file for all NILs and CSSs mentioned in this manuscript. File S9 contains each of the 97 significant PCs and the corresponding correlation value with each growth-response trait. File S10 contains the residual phenotypic data for all strains, including parents, tested in the NIL and CSS assays. File S11 contains the statistical significance for all pairwise combinations of strains tested for each trait in the NIL and CSS assays. File S12 contains the assay categorization for all traits tested with the NIL and CSS strains. The data sets and code for generating figures can be found at http:// github.com/AndersenLab/QTLhotspot Supplemental material available at Figshare: https://doi.org/10.25386/genetics.7158911.

Results

Identification of QTL underlying variation in response to 16 diverse toxins

Using a high-throughput fitness assay (*Materials and Methods*), we tested variation in 24 fitness-related traits in responses of four genetically divergent strains to different concentrations of 16 toxins, comprising chemotherapeutics, heavy metals, pesticides, and neuropharmaceuticals (Figure S1, File S1, and Table S1). A concentration of each toxin was selected that minimized within-strain variation and maximized variation between two of these divergent strains, N2

Table 3 Categorization summary from NIL phenotypes

Primary category	Number of tests (99)
No parental effect	23
Recapitulation	4
No QTL effect	11
Unidirectional transgressive	38
Bidirectional transgressive	7
Miscellaneous	16

(the laboratory strain) and CB4856 (a wild isolate from Hawaii) (Table S1). For the selected concentration of each toxin, we assayed 24 growth-response traits for a panel of 296 RIAILs generated between the N2 and CB4856 parental genetic backgrounds (File S2) (Andersen *et al.* 2015). We then performed linkage mapping for each of the 24 traits across each of the 16 toxins, for a total of 384 toxin-trait mappings. Through this method, we identified 462 QTL across 247 traits (Figure S2 and File S3). However, many of the toxin-response traits are correlated (Figure S3), which could result in an increased detection of false-positive QTL. To account for this bias, we performed principal component analysis (PCA) for each toxin. The minimum number of principal components (PCs) that explained at least 90% of the total phenotypic variance within each toxin was selected for mapping, for a total of 97 PCs across all toxins (minimum of five PCs and a maximum of eight PCs per toxin, File S4 and Table S2). We then used linkage mapping to identify QTL that underlie variation in these 97 PCs.

We detected a total of 82 significant QTL (across 47 PCs) from the 97 PCs tested (Figure 1, Figure S4, and File S5). We did not find a single toxin-response QTL shared robustly across all of the various PCs and toxins tested, nor across all PCs within any one toxin. However, the majority of the QTL on chromosome I were detected in responses to chemotherapeutics. Additionally, almost every toxin (with the exception of FUdR) had QTL that underlie trait variation on at least two different chromosomes, highlighting the diverse architectures implicated across traits, even within a single toxin. Despite the seemingly independent distributions of QTL, we found that the majority of the QTL (61%) mapped to chromosomes IV and V.

Both additive and interactive QTL underlie toxin responses

For each of the PCs that were impacted by the 82 QTL identified using linkage mapping, we calculated the broad-sense heritability, the proportion of broad-sense heritability that could be attributed to additive genetic components (narrow-sense heritability) (Figure 2A), and the proportion of narrow-sense heritability that was explained by QTL detected through linkage mapping (Figure 2B and File S7, *Materials and Methods*). In many cases, additive genetic components could not explain all of the phenotypic variation predicted to be caused by genetic factors. These results suggest that other additive loci with small effect sizes impact toxin responses, but we failed to detect these QTL by our linkage mapping analyses, potentially because of high complexity and/or insufficient statistical power. Alternatively, this missing heritability could be indicative of genetic interactions (Bloom *et al.* 2013).

To determine how much of the phenotypic variance comes from additive or interacting genetic components, we fitted a linear mixed-effect model to the RIAIL phenotype data for the 47 PCs controlled by the 82 QTL. We observed a range of additive and epistatic components contributing to phenotypic variation across toxin classes (Figure S4, Figure S5, and File S7). On average, cisplatin, topotecan, and FUdR are primarily explained by additive models (Figure S4). Alternatively, paraquat, irinotecan, vincristine, and mechlorethamine have a larger fraction of their phenotypic variance attributable to genetic interactions than additive effects (Figure S4). To localize potential genetic interactions for these 82 QTL, we scanned the genome for interactions between pairs of markers that might affect the phenotypic distribution of the RIAIL panel (*Materials and Methods*). We identified three significant interactions (File S6). This two-factor genome scan was unable to localize all epistatic components identified by the linear mixed-effect model (Figure 2), perhaps because of missing small-effect additive loci in the model and/or insufficient statistical power to identify small-effect interactions.

Three QTL hotspots underlie variation in responses to diverse toxins

The majority of toxin-response QTL cluster on chromosomes IV and V (Figure 1). We sought to determine if such QTL clustering could be expected by chance or if this clustering is indicative of toxin-response QTL hotspots. To account for the higher rate of recombination, and thus more genetic diversity, on the chromosome arms (Rockman and Kruglyak 2009), we divided the genome evenly into 65 bins and calculated the number of QTL that mapped to each bin (Figure 3, *Materials and Methods*). Three bins with more QTL than expected based on a Poisson distribution (Brem and Kruglyak 2005) were classified as hotspots. These hotspots are located on the center of chromosome IV, the right of chromosome IV, and the center of chromosome V, and are hereby denoted as IVL, IVR, and V, respectively. We identified the same three hotspots through analysis of linkage mapping results from toxin-response phenotypes that were used to calculate PCs. Importantly, these hotspots are not driven by multiple PCs within a single toxin. Instead, hotspots comprise multiple QTL across a variety of PCs and toxins. In fact, 14 of the 16 toxins tested have a PC that maps to at least one of the three hotspots (Table 1). Of the 82 QTL, 18 mapped to IVL, eight mapped to IVR, and nine mapped to V. In total, 33 QTL map to a hotspot (note that two QTL have confidence intervals that span both hotspots on chromosome IV). We sought to experimentally validate the predicted additive and epistatic effects on toxin responses for QTL that mapped to the three hotspots.

NILs recapitulate some of the predicted QTL effects

To experimentally validate the QTL identified from linkage mapping, we created NILs for the IVL, IVR, and V hotspots.

Table 4 Categorization summary from combined NIL and CSS phenotypes

Secondary Category	Number of Traits (8)	Traits
Recapitulation	1	cisplatin.norm.n
Interchromosomal (external)	1	silver.median.TOF (bidirectional)
Interchromosomal (internal)	1	carmustine.median.EXT (unidirectional)
Intrachromosomal	2	cisplatin.q90.EXT (unidirectional), cisplatin.q90.TOF (unidirectional)
Miscellaneous	3	cisplatin.n, paraquat.q10.TOF, silver.median.EXT

EXT, extinction; TOF, time of flight.

Each NIL has a small genomic region introgressed from one parental strain into the genome of the opposite parental strain (*Materials and Methods*). These NILs were whole-genome sequenced and found to match the expected genotype in the hotspot region; however, additional breakpoints were observed (*Material and Methods*, File S8). We tested each NIL in our high-throughput fitness assay for a subset of the toxins with a QTL that maps to a given hotspot, choosing QTL with small, medium, and large effect sizes to test our ability to recapitulate various effect sizes (Table S4, Table 1, and Table 2). We tested five toxins (10 QTL) with the IVL NILs, three toxins (four QTL) with the IVR NILs, and five toxins (six QTL) with the V NILs. In total, we tested 20 QTL across eight toxins for recapitulation using the NILs.

For each of these 20 QTL, we identified the toxin-response trait that is most correlated with the PC controlled by that QTL. We then assayed the NILs for that toxin-response trait as well as all toxin-response traits within its same trait cluster, because each PC comprises multiple toxin-response traits (Table 2, *Materials and Methods*). We tested 42 toxin-response traits with the IVL NILs, 12 toxin-response traits with the IVR NILs, and 45 toxin-response traits with the V NILs (Figure S6, File S10, and Table 2). In total, we performed 99 tests of recapitulation of QTL effects for toxin-response traits. The results of these tests allowed us to sort QTL effects into six different categories: "no parental effect", "recapitulation", "no QTL effect", "unidirectional transgressive," "bidirectional transgressive," or "miscellaneous" (Figure S7, File S12, and Table 3).

Of these 99 tests, 23 did not display a significant phenotypic difference between the parent strains (N2 and CB4856) in the NIL assay and were categorized as "no parental effect" (*Materials and Methods*, Figure S6 and Table 3). The remaining 76 tests in which a significant parental difference was observed were classified further. We predicted that if a single QTL in the introgressed region contributed to the parental phenotypic difference, then each NIL would have a phenotype significantly different from the parental strain with the same genetic background. Furthermore, we expected each NIL to have a phenotype similar to the parental strain of its introgressed genomic region. This "recapitulation" model was consistent for four tests (Figure S6 and Table 3). The normalized brood size trait in cisplatin (cisplatin.norm.n in cisplatin PC4) is one such example of a trait in which the NILs on the center of chromosome V recapitulated the expected parental phenotype (Figure 4A). For 11 of the remaining 72 tests, the phenotype of each NIL was not significantly different from the phenotype of the parental strain sharing its background genotype (Figure S6 and Table 3). This phenotype indicates that the introgressed NIL region was not affecting the toxin-response phenotype. This lack of QTL effect suggests that the genetic architecture is more complex, we lacked sufficient statistical power to detect the QTL effect, or the real QTL is outside the introgressed region. The NILs on the center of chromosome V showed this result for median animal length in silver (silver.median.TOF in silver PC1) (Figure 4B). The phenotypes of the NILs for the remaining 61 tests cannot be explained by a single-QTL model. For many of these tests, we observed NIL phenotypes that are more sensitive or more resistant than both parental strains, suggesting that loci of opposite genotypes act additively or interact in the NILs to create transgressive phenotypes (Dittrich-Reed and Fitzpatrick 2013). This finding was supported by the mixed-effects model, which suggested that both additive and interacting QTL remained undetected by linkage mapping (Figure 2). We further explored the results of these 61 tests by characterizing them based on the patterns of the transgressive phenotypes we observed.

For 38 of these 61 tests, only one NIL showed a transgressive phenotype (Figure S6 and Table 3). Some of these 38 "unidirectional transgressive" phenotypes seem to show an antagonism that counteracted the effect of the introgressed region (a predicted sensitive phenotype becomes hyperresistant or a predicted resistant phenotype becomes hypersensitive, *e.g.*, carmustine.median.EXT in carmustine PC1, Figure 4C). Other phenotypes displayed synergy that increased the effect of the introgressed region (a predicted sensitive phenotype becomes a hypersensitive phenotype or a predicted resistant phenotype becomes a hyperresistant phenotype, *e.g.*, cisplatin.q90.EXT in cisplatin PC1, Figure 4D). Interestingly, in most cases (82%), the transgressive phenotype was observed in the strain with the N2 genotype introgressed into the CB4856 background.

In addition to unidirectional transgressive phenotypes, we identified seven tests with suggested "bidirectional transgressive" phenotypes in which both NILs showed an extreme phenotype compared to the parental strains (Figure S6 and Table 3). Some of these "bidirectional transgressive" phenotypes were suggestive of purely antagonistic effects (*e.g.*, tunicamycin.mean.norm.EXT, Figure S6), but others suggested an antagonistic effect in one NIL and a synergistic effect in the other (*e.g.*, paraquat.median.TOF, Figure S6). We identified no cases of bidirectional synergistic effects. The remaining 16 tests of the 76 with a parental difference did not fall into any of the above categories and were classified as "miscellaneous" (Table 3).

The toxin-response traits tested above for recapitulation of QTL effects were selected to represent PCs that were mapped

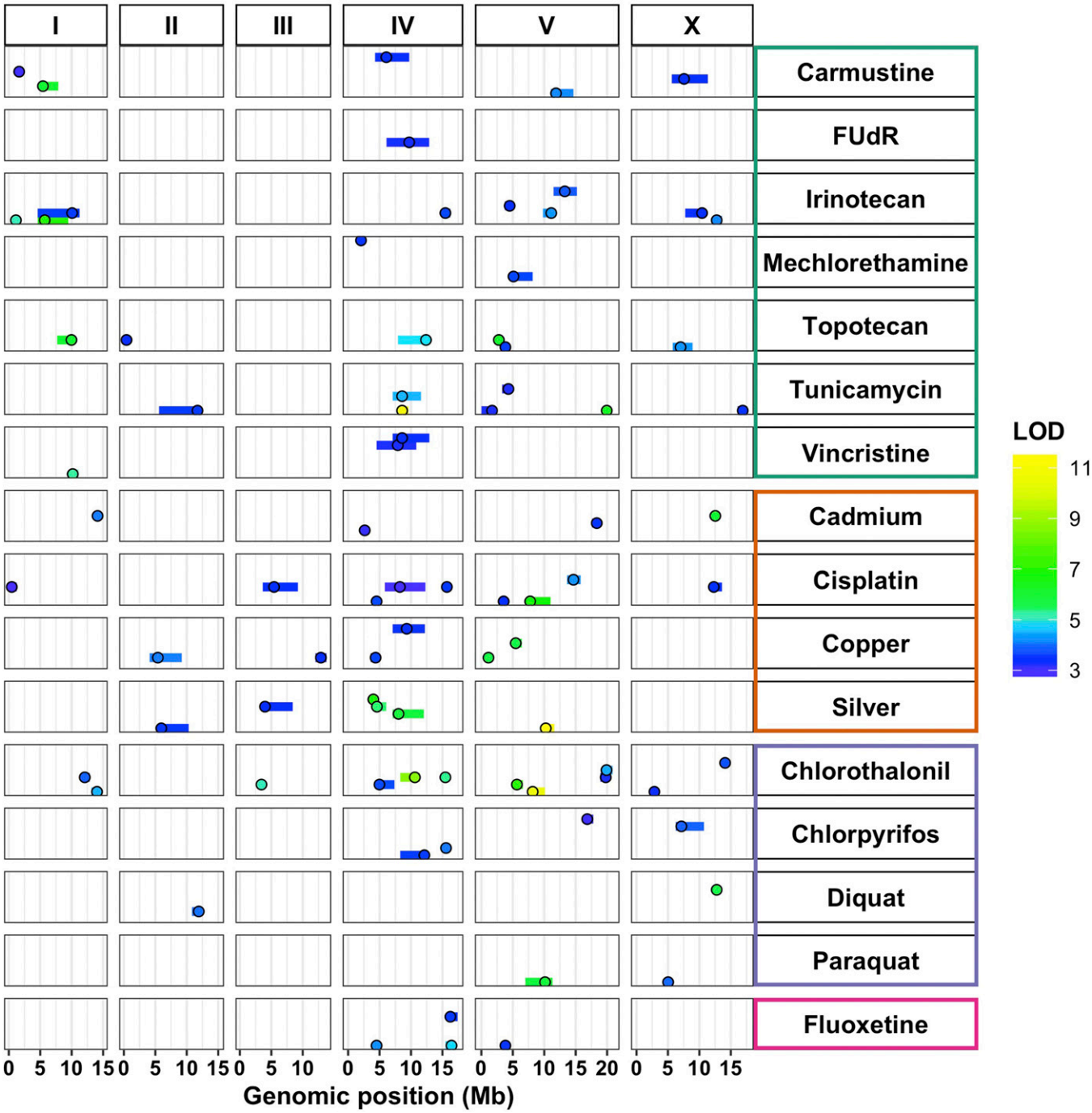

Figure 1 Diverse genetic architectures are implicated in responses to 16 toxins. Linkage mapping results for principal components that represent 82 QTL across 16 toxins, comprising chemotherapeutics (teal), heavy metals (orange), pesticides (purple), and neuropharmaceuticals (pink) are plotted. Genomic position (Megabase) is shown along the *x*-axis, split by chromosome, and each of the 47 principal components with a significant QTL is plotted along the *y*-axis. Each QTL is plotted as a point at the location of the most significant genetic marker and a line indicating the 95% C.I. QTL are colored by the logarithm of the odds (LOD) score, increasing in significance from blue to green to yellow. FUdR, floxuridine.

with linkage mapping. We wanted to compare the NIL assay categorizations for the toxin-response traits that underlie each PC to analyze the overall QTL effect (Figure S8). For example, two traits, n and norm.n, were selected to represent cisplatin PC4 (Table 2). Both of these toxin-response traits were placed into the "recapitulation" category from the NIL assay results (Figure S6 and Figure S8). These results suggest that a single additive QTL underlies the brood size variation captured by PC4. Fourteen tunicamycin-response traits were selected to represent tunicamycin PC1 (Table 2). Eight of these 14 traits displayed "unidirectional transgressive phenotypes", four traits displayed "bidirectional transgressive

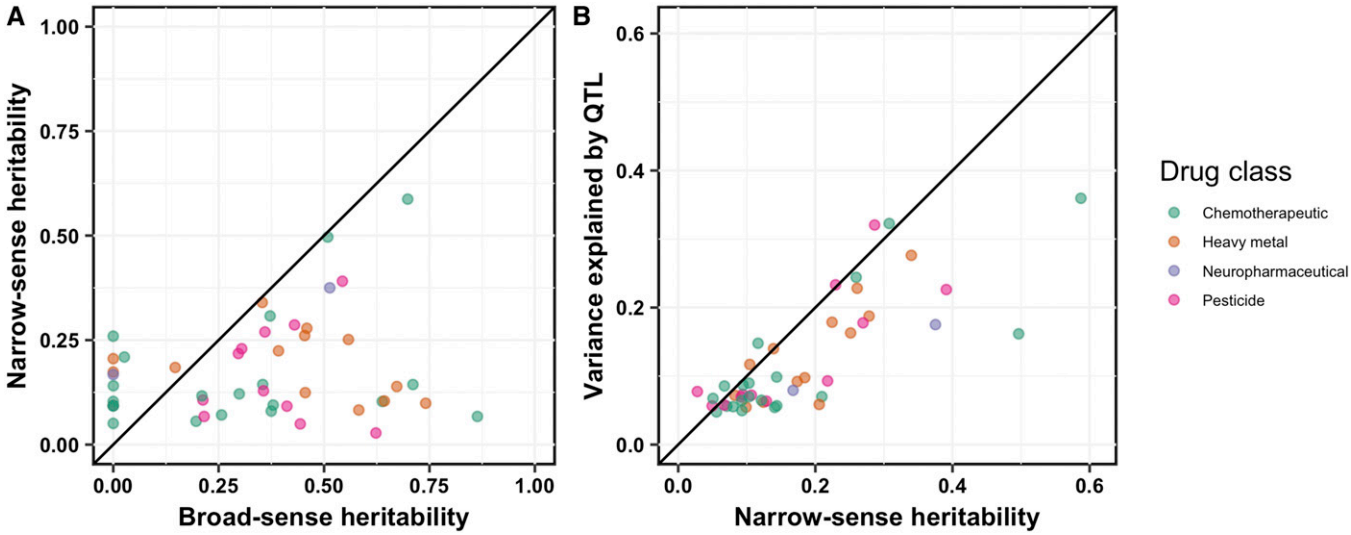

Figure 2 Additive genetic components identified by linkage mapping do not explain all heritable contributions to toxin-response variation. For 47 principal components representing the 82 QTL, we compared (A) the broad-sense heritability (*x*-axis) calculated from the recombinant inbred advanced intercross line phenotypic data *vs.* the narrow-sense heritability (*y*-axis) estimated by a mixed model, and (B) the narrow-sense heritability (*x*-axis) *vs.* the variance explained by all QTL detected by linkage mapping (*y*-axis). In both plots, each principal component is plotted as a point whose color indicates drug class (chemotherapeutic, heavy metal, neuropharmaceutical, or pesticide). The diagonal line represents y = x and is shown as a visual guide.

phenotypes", and the remaining two traits did not have a significant parental phenotypic difference (Figure S6 and Figure S8). Regardless of the classification, we see the same trend of resistance (ECA231 > N2 > CB4856 > ECA229) across 11 of the 14 traits representing this PC. Therefore, our strict significance thresholds for categorization might have caused some phenotypes to be miscategorized (usually into the "miscellaneous" or "no parental/QTL effect" categories). The prevalence of transgressive phenotypes in tunicamycin-response traits suggests that multiple QTL, acting additively or interacting, might impact tunicamycin responses.

We next sought to compare categorizations of toxin-response traits and QTL effect sizes of the PCs for those traits. The QTL underlying cisplatin PC4 explains ~7% of the total phenotypic variance (Table S4). The traits selected to represent cisplatin PC4 were placed into the recapitulation category, despite the small effect size of the QTL (Figure S6 and Figure S8). In the other example above, the QTL underlying tunicamycin PC1 explains almost 16% of the total phenotypic variance, which is one of the highest effect sizes mapped in this study (Table S4). The toxin-response traits selected to represent this PC showed mostly transgressive phenotypes, indicating undetected additive or interacting QTL despite the seemingly large-effect additive QTL identified in linkage mapping (Figure S6 and Figure S8).

CSSs localize QTL underlying transgressive phenotypes

Because we found evidence of loci where opposite genotypes at each locus cause transgressive phenotypes, we attempted to further characterize these loci (Figure 5 and Figure S7). To define each set of loci as either "intrachromosomal" or "interchromosomal", we built reciprocal CSSs for the hotspot on chromosome V that had the entire chromosome V introgressed from one parental strain into the genome of the opposite parental strain (*Materials and Methods*). The hotspot on chromosome V was chosen to isolate the effects of one hotspot and avoid complications arising from traits whose confidence intervals might lie within both of the hotspots on chromosome IV. The CSSs were whole-genome sequenced and found to have the expected genotype at all markers (*Materials and Methods*, File S8), except for the chromosome I incompatibility locus (Seidel *et al.* 2008, 2011). We performed tests of recapitulation of QTL effects with the CSSs for each of the 45 toxin-response traits across the five toxins tested with the chromosome V NILs (Figure S6, File S10, Table S4, and Table 2).

For traits in which the parental phenotypic difference was significant and consistent across the NIL and CSS tests, NIL and CSS phenotypes could be compared across assays. Eight traits across five toxins fit this criterion (File S12 and Table 4). One trait (cisplatin.norm.n) displayed phenotypic recapitulation of the introgressed region in both the NIL and the CSS tests, suggesting a single-QTL model (Figure 4A and Table 4). Alternatively, transgressive phenotypes are indicative of a multi-QTL model, and locations of additive or interacting QTL can be surmised by comparing results from the NIL and CSS tests. Transgressive phenotypes controlled by interchromosomal loci are defined by two loci on separate chromosomes that act additively or epistatically. Because NILs and CSSs have introgressed genotypes on chromosome V, we can deduce that at least one of the two interchromosomal loci is located on chromosome V. We further divided the interchromosomal class into two categories: "interchromosomal external," in which the

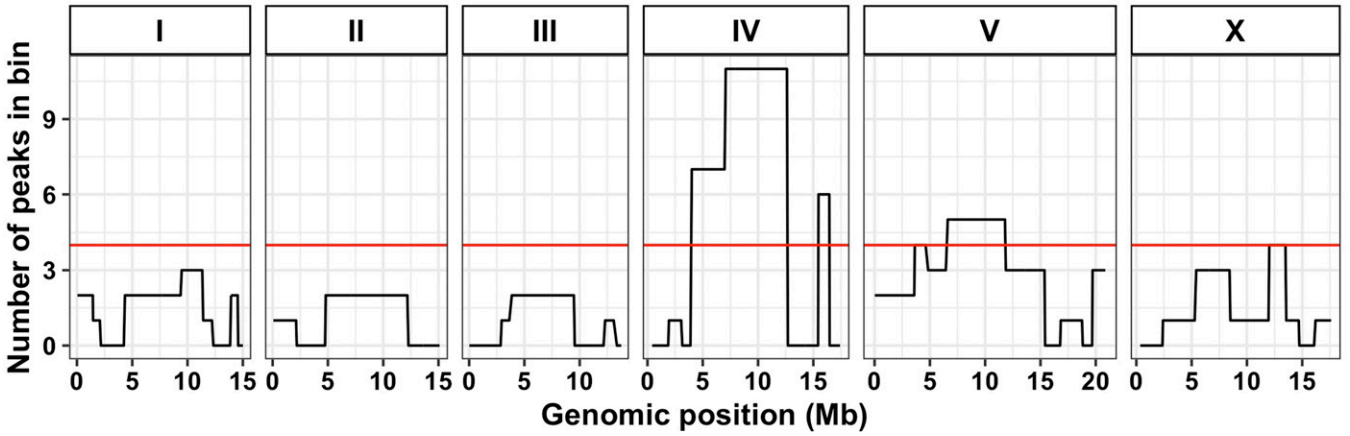

Figure 3 Three QTL hotspots impact toxin responses. Each chromosome is divided into equal bins of 26 cM, resulting in a total of 65 bins across the genome. The *x*-axis shows the genomic position (Megabase) and the *y*-axis shows the number of QTL that lie within the corresponding bin. The red line indicates the 99th percentile of a Poisson distribution with a mean of 1.26 QTL (total QTL/total bins).

chromosome V locus is outside the region introgressed in the NILs (Figure 5A), and "interchromosomal internal," in which the chromosome V locus is within the region introgressed in the NILs (Figure 5B). For an "interchromosomal external" model, we expect only the CSSs to display hypersensitivity or hyperresistance, because both loci share the same genotype in the NILs (Figure 5A) and would therefore not result in a more extreme phenotype than both parents. We found one such trait that fits a "bidirectional interchromosomal external" loci model (silver.median.TOF) (Figure 4B and Table 4). For an "interchromosomal internal" model, we expected both the CSSs and the NILs to display the same hypersensitivity or hyperresistance, because both strains share the same genotype across the introgressed region in the NILs (Figure 5B). We identified one such trait that fits a "unidirectional interchromosomal internal" loci model (carmustine.median.EXT) (Figure 4C and Table 4). To identify intrachromosomal loci that underlie transgressive phenotypes in the remaining 10 traits, we searched for traits that display evidence of either a uni- or bidirectional transgressive phenotype in the NILs but not in the CSSs (Figure 5C). This result would suggest that two loci of opposite genotypes on chromosome V, one within and one outside the region introgressed in the NILs, act additively or epistatically to cause transgressive phenotypes. We found two examples of such "unidirectional intrachromosomal" loci models (*e.g.*, cisplatin.q90.EXT, Figure 4D and Table 4). The remaining three traits could not be characterized beyond their NIL assay characterization based on the results of the CSS assay (Table 4).

We revisited the two-factor genome scan results for each of these eight empirically classified traits and compared the findings from these two independent methods used to identify multiple additive or epistatic QTL. No traits with significant interaction terms were identified by the two-factor genome scan. Although many other pairs of loci show suggestive evidence of additive or interacting effects (File S5), an increase in statistical power is required to definitively compare these suggestive findings to our empirically derived model. Overall, this study highlights the benefits of leveraging both experimental and computational strategies to further dissect genetic components that underlie quantitative traits in a metazoan model.

Discussion

Here, we show that three QTL hotspots underlie differences in responses to 16 diverse toxins. We further characterized these QTL using both modeling and empirical approaches. Through the use of NILs and CSSs, we confirmed small-effect QTL, and attempted to identify and localize genomic regions causing transgressive phenotypes. Finally, we used statistical analyses to computationally identify loci that might support some of our empirical findings. Although the number of biological replicates and recombinant strains in this study increased our power to detect QTL compared to previous studies, we are still too underpowered to definitively assess if missing heritability is composed of small additive effects or genetic interactions.

Pleiotropic regions underlie QTL shared between and among toxin classes

We performed PC analysis on toxin-response phenotypes collected for a panel of RIAILs and used linkage mapping to identify 82 toxin-response QTL. Although some of these QTL are unique to one particular toxin, others suggest the existence of pleiotropic QTL that underlie responses to a diverse set of toxins. In particular, three QTL hotspots across chromosomes IV and V were enriched for toxin-response QTL, and were investigated further. Because the molecular mechanisms implicated in responses to each toxin differ drastically, the notion that a single gene in each hotspot is regulating the response to several toxins is unlikely. However, the possibility exists that a single gene involved in drug transport could underlie one or several of these hotspots. More likely, multiple genes in close proximity, each regulating a process controlling cellular proliferation and survival, might underlie these hotspots. Notably, two of the three QTL hotspots are in swept regions with lower genetic diversity at the species level (Andersen *et al.* 2012;

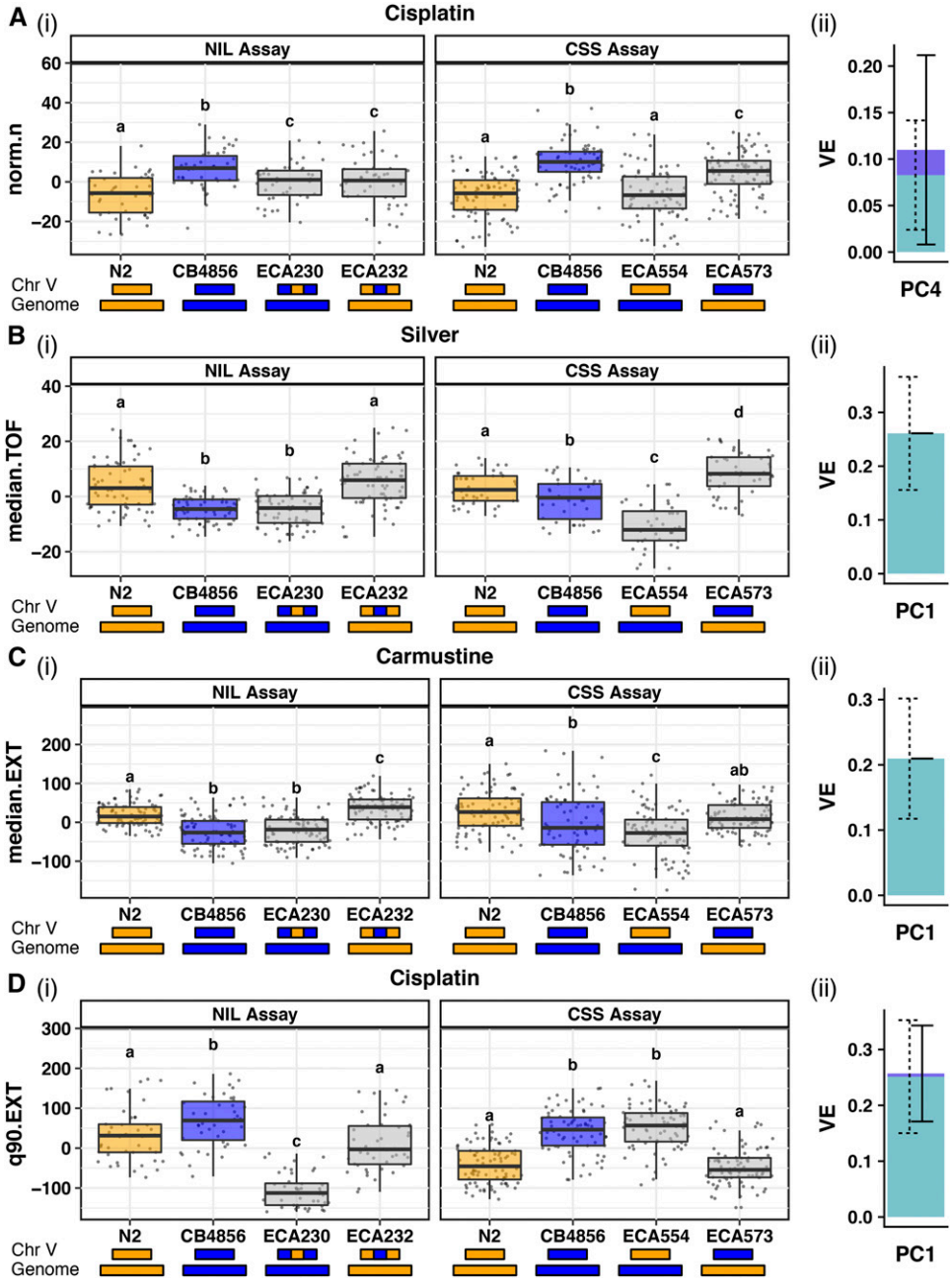

Figure 4 Results from NIL and CSS tests of recapitulation of QTL effects are categorized based on potential genetic mechanisms implicated in toxin responses. A trait contributing to a mapped PC for each category is reported: (A) Recapitulation (cisplatin norm.n, PC4), (B) interchromosomal external bidirectional loci (silver median.TOF, PC1), (C) interchromosomal internal unidirectional loci (carmustine median.EXT, PC1), and (D) intrachromosomal unidirectional loci (cisplatin q90.EXT, PC1). In each case, we show results from (i) the NIL assay (left) and CSS assay (right) plotted as Tukey box plots. The *y*-axis indicates residual phenotypic values for the given trait. Different letters (a–d) above each Tukey box plot represent significant differences ($P < 0.05$), while the same letter represents nonsignificant differences between two strains (Tukey's honest significant difference). The genotype of each strain on the *x*-axis is modeled by the colored rectangles beneath the plots (N2 genotypes are orange and CB4856 genotypes are blue). (ii) A stacked bar plot shows the proportion of phenotypic variation attributable to additive (light blue with dashed error bars) and interactive (dark blue with solid error bars) genetic factors of the PC represented by each trait, based on a mixed model. Chr, chromosome; CSS, chromosome substitution strain; EXT, extinction; NIL, near-isogenic line; PC, principal component; TOF, time of flight; VE, variance explained estimate.

Cook *et al.* 2016, 2017; Laricchia *et al.* 2017). The laboratory strain, N2, has experienced each of the selective sweeps, and CB4856 has not. Linkage mapping using a panel of RIAILs built between these two strains could identify QTL that underlie phenotypic differences between swept and nonswept strains. Moreover, identifying QTL in these swept regions that underlie variation in fitness-related traits might indicate selective pressures that could have led to these chromosomal sweeps. For example, N2 is more resistant than CB4856 to tunicamycin (Figure S6), an antibiotic and chemotherapeutic produced by the soil bacterium *Streptomyces clavuligerus* (Price and Tsvetanova 2007). This result might suggest that selective pressure toward responses to antibiotic compounds played a role in driving resistance-conferring alleles, such as those present in N2, to a high frequency. Alternatively, climate conditions could also impact local niche environments to sensitize toxin responses (Evans *et al.* 2017). We observed that N2 is more resistant than CB4856 in responses to the majority of conditions, which could indicate that alleles present in swept strains confer robustness in responses to many conditions. This result emphasizes the importance of genetic background when considering toxin effects (Zdraljevic and Andersen 2017).

In addition to the three QTL hotspots, pleiotropic QTL across toxins within certain classes are suggested by our linkage mapping results. We observed an enrichment of QTL from the chemotherapeutic class on chromosome I, which could be representative of QTL that underlie a common

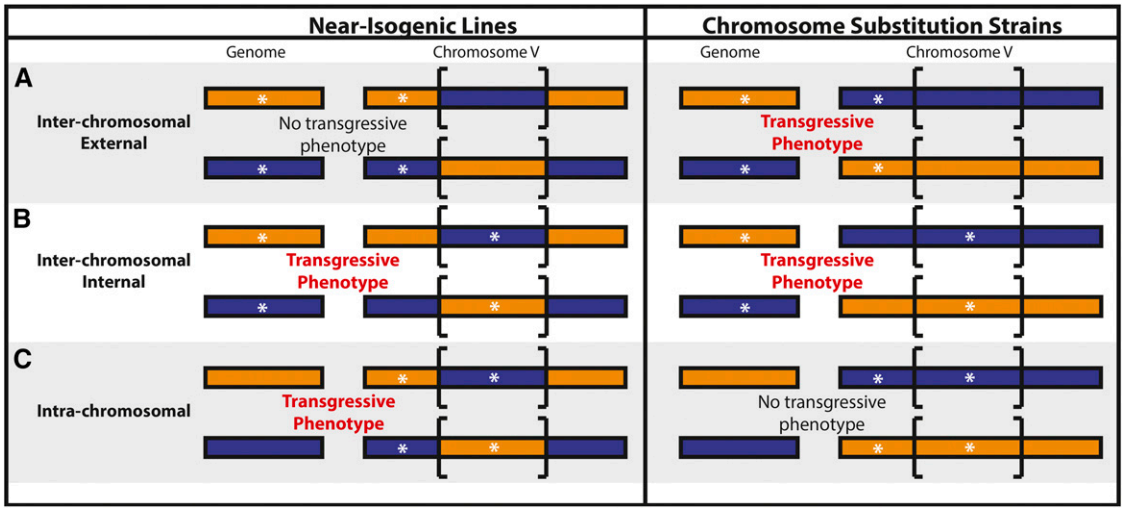

Figure 5 A model for potential locations of two loci is shown, according to toxin-response phenotypes of near-isogenic lines (NILs) and chromosome substitution strains (CSSs). The NILs are represented on the left and the CSSs are represented on the right. The strain genotype is indicated by colored rectangles. N2 is orange and CB4856 is blue. Brackets indicate the genomic region that is introgressed in the NILs. White asterisks represent a potential location for additive or epistatic loci underlying transgressive phenotypes. Although bidirectional transgressive phenotype models are shown, each model could be bidirectional (both reciprocal introgressed strains show transgressive phenotypes) or unidirectional (only one reciprocal introgressed strain shows a transgressive phenotype). Models showing (A) interchromosomal external effects between a locus outside of the introgressed region in the NILs and a locus on another chromosome, (B) interchromosomal internal effects between a locus within the introgressed region in the NILs and a locus on another chromosome, and (C) intrachromosomal effects between a locus within and a locus outside of the introgressed region in the NILs are drawn.

mechanism targeted by these toxins, such as DNA damage or cell-cycle control. However, because many of these chemotherapeutics have distinct mechanisms of action and share these mechanisms with other toxin classes, this enrichment is likely caused by an overrepresentation of chemotherapeutics in our study. Direct comparisons of toxins with similar cellular mechanisms could provide more insights. For example, irinotecan and topotecan are both chemotherapeutics that cause DNA damage by inhibiting topoisomerase I (Pommier 2006), and share a QTL on the center of chromosome I. However, each of these chemotherapeutics also maps to distinct regions of the genome. For example, the irinotecan-response QTL on the right arm of chromosome V is not mapped for topotecan response and the topotecan-response QTL on the left arm of chromosome II is not mapped for irinotecan response. Vincristine also maps to this same region; however, its mechanism of action is distinct from irinotecan and topotecan. The combination of overlapping and distinct genetic architectures underlying these highly similar compounds suggest that although some genetic variation implicated in responses to irinotecan and topotecan is shared, other QTL are specific to each compound and not representative of a general topoisomerase I inhibition mechanism. We have also observed this phenomenon of distinct genetic architectures underlying similar compounds for benzimidazole responses (Zamanian *et al.* 2018).

A multi-faceted approach suggests that undetected epistatic loci impact toxin responses

To determine if we had sufficient power to experimentally validate even small-effect QTL, we constructed NILs for the three hotspots and assayed them in responses to multiple toxins. Because each PC comprises multiple toxin-response traits, we measured NIL phenotypes for the most correlated toxin-response traits for each PC to test recapitulation of QTL effects. For some of these tests of recapitulation for small-effect QTL, NILs showed a significant phenotypic effect. One such example is cisplatin.norm.n and cisplatin.n, which represent the QTL mapped by cisplatin.PC4 that only explain 7% of the phenotypic variance. Our ability to recapitulate such a small effect suggests that our assay had sufficient power to detect small phenotypic effects in at least some cases. We postulated that our inability to recapitulate other QTL effects could be attributed to either insufficient power or additional additive or epistatic QTL that were undetected by linkage mapping. Particularly in cases where the NILs displayed transgressive phenotypes, undetected loci of opposite genotypes, acting additively or epistatically, likely caused these effects. Therefore, we investigated these interactions and found evidence for additional QTL that interact with the originally detected loci. However, we must note that whole-genome sequence data revealed that three of our NILs had a portion of the genome from the background of the starting RIAIL (File S7). Although we do not believe that these small regions are responsible for the unexpected phenotypes observed, this explanation could be a consideration for certain silver, cisplatin, carmustine, and chlorothalonil PCs, as they have significant QTL in these identified regions. This example emphasizes the importance of whole-genome sequencing NILs to verify the expected genotypes before making conclusions about phenotypic effects of a targeted QTL.

We used the results from the NIL assays to classify each test into a category that predicts a genetic model that might underlie NIL phenotypes. Categorizations were consistent across traits representing a PC, with most of these traits falling into one or a few categorizations. This widespread consistency suggests that similar genetic architectures underlie phenotypes for these grouped traits. Furthermore, this consistency highlights the reproducibility of our high-throughput toxin-response assay, because results from independent assays (trait correlations, linkage mappings from RIAIL assays, and phenotype classifications from NIL assays) often align to support the same conclusion obtained from the individual experiments.

The majority of cases of transgressive phenotypes occur when the N2 genotype is introgressed into the CB4856 genome. This trend might indicate allele-specific unidirectional incompatibilities between the two strains, and localizing these interactions could improve our understanding of the evolutionary processes driving such incompatibilities. However, identifying the loci that underlie these unidirectional transgressive phenotypes using a mixed-effect model or a two-factor genomic scan is difficult, because only a small number of the RIAILs have the required allelic combinations to quantify such an effect. For example, cisplatin.q90.EXT, a trait chosen to represent cisplatin PC1, fits a unidirectional intrachromosomal model. The results of the NIL and CSS assays show that, although the CSSs seem to display no QTL effect, the NIL with the N2 genotype introgressed into the CB4856 genome displays strong hypersensitivity (Figure 4D). All of the narrow-sense heritability for cisplatin PC1 (25%) predicted by the mixed-effect model is explained by the three QTL identified through linkage mapping (the variance explained estimates of these three QTL add up to 26%, File S5 and File S7). This finding suggests that most of the additive loci have been identified through linkage mapping. Therefore, the intrachromosomal loci are likely acting epistatically to cause a unidirectional transgressive phenotype. However, using our mixed-model approach, we do not find a significant interaction component for cisplatin PC1, the PC that is represented by cisplatin.q90.EXT. A two-dimensional genome scan for multiple loci that underlie cisplatin PC1 provides suggestive evidence for a two-QTL model over a one-QTL model, with or without interaction between the loci (File S6). These two loci are located on the left of chromosome V (outside the NIL interval) and in the center of chromosome V (inside the NIL interval), and match our empirical evidence of two intrachromosomal loci underlying the transgressive phenotype observed (Figure 5C). Because the transgressive phenotype is unidirectional, RIAILs without the allelic combination that causes extreme phenotypes could dilute our power to detect the loci. For this reason, combining both computational models and empirical investigation facilitates the detection of loci that control transgressive phenotypes. Additionally, future studies should include even larger RIAIL panels than what we used here to empower approaches to investigate the contributions of interactive loci.

Although we are statistically underpowered to identify some small-effect additive and interacting loci through modeling, the combination of three methods of searching for potential interactions suggests that not all fitness traits in *C. elegans* are composed of additive effects. Our two computational methods were used to identify additive and epistatic loci underlying many toxin responses, but their power was limited in cases of unidirectional transgressive phenotypes. Alternatively, the NIL and CSS phenotypic assays were able to identify unidirectional transgressive phenotypes, but they were restricted by their inability to distinguish between additive and epistatic loci. Constructing double CSS strains or multi-region NILs in which pairwise combinations of two genomic regions are introgressed within the opposite genotype could help to further define loci underlying transgressive phenotypes. However, each locus must be isolated to determine if the two loci act additively or epistatically. The results from the two-dimensional genome scan might provide insights into where to begin this approach. In cases where all three of our techniques suggested epistasis, we suspect that these QTL are not purely additive. Generating an even larger panel of recombinant strains and assaying a much larger number of biological replicates might allow us to further address the debate about how heritable loci contribute to trait variation in metazoans.

Acknowledgments

The authors would like to thank Bryn Gaertner, Samuel Rosenberg, and Tyler Shimko, for assistance with mapping drug sensitivities, and members of the Andersen laboratory for helpful comments on this manuscript. This work was supported by the following grants to E.C.A.: National Institutes of Health R01 subcontract to E.C.A. (GM-107227), the Chicago Biomedical Consortium with support from the Searle Funds at the Chicago Community Trust, and an American Cancer Society Research Scholar Award (127313- RSG-15-135-01-DD). S.C.B. was supported by a Biotechnology Training grant (T32 GM-008449). K.S.E. was supported by the Cell and Molecular Basis of Disease Training grant (T32 GM-008061). J.S.B. was supported by the Howard Hughes Medical Institute. The funders had no role in study design, data collection and analysis, the decision to publish, or preparation of the manuscript.

Literature Cited

Altshuler, D., M. J. Daly, and E. S. Lander, 2008 Genetic mapping in human Disease. Science 322: 881–888. https://doi.org/10.1126/science.1156409

Andersen, E. C., J. P. Gerke, J. A. Shapiro, J. R. Crissman, R. Ghosh *et al.*, 2012 Chromosome-scale selective sweeps shape Caenorhabditis elegans genomic diversity. Nat. Genet. 44: 285–290. https://doi.org/10.1038/ng.1050

Andersen, E. C., J. S. Bloom, J. P. Gerke, and L. Kruglyak, 2014 A variant in the neuropeptide receptor Npr-1 is a major determinant of Caenorhabditis elegans growth and physiology. PLoS

Genet 10: e1004156. https://doi.org/10.1371/journal.pgen.1004156

Andersen, E. C., T. C. Shimko, J. R. Crissman, R. Ghosh, J. S. Bloom *et al.*, 2015 A powerful new quantitative genetics platform, combining Caenorhabditis elegans high-throughput fitness assays with a large collection of recombinant strains. G3 (Bethesda) 5: 911–920. https://doi.org/10.1534/g3.115.017178

Balla, K. M., E. C. Andersen, L. Kruglyak, and E. R. Troemel, 2015 A wild C. elegans strain has enhanced epithelial immunity to a natural microsporidian parasite. PLoS Pathog. 11: e1004583. https://doi.org/10.1371/journal.ppat.1004583

Bendesky, A., and C. I. Bargmann, 2011 Genetic contributions to behavioural diversity at the gene-environment interface. Nat. Rev. Genet. 12: 809–820. https://doi.org/10.1038/nrg3065

Bendesky, A., M. Tsunozaki, M. V. Rockman, L. Kruglyak, and C. I. Bargmann, 2011 Catecholamine receptor polymorphisms affect decision-making in C. elegans. Nature 472: 313–318. https://doi.org/10.1038/nature09821

Bendesky, A., J. Pitts, M. V. Rockman, W. C. Chen, M.-W. Tan *et al.*, 2012 Long-range regulatory polymorphisms affecting a GABA receptor constitute a quantitative trait locus (QTL) for social behavior in Caenorhabditis elegans. PLoS Genet. 8: e1003157. https://doi.org/10.1371/journal.pgen.1003157

Bloom, J. S., I. M. Ehrenreich, W. T. Loo, T.-L. V. Lite, and L. Kruglyak, 2013 Finding the sources of missing heritability in a yeast cross. Nature 494: 234–237. https://doi.org/10.1038/nature11867

Bloom, J. S., I. Kotenko, M. J. Sadhu, S. Treusch, F. W. Albert *et al.*, 2015 Genetic interactions contribute less than additive effects to quantitative trait variation in yeast. Nat. Commun. 6: 8712. https://doi.org/10.1038/ncomms9712

Boyd, W. A., M. V. Smith, and J. H. Freedman, 2012 Caenorhabditis elegans as a model in developmental toxicology. Methods Mol. Biol. 889: 15–24. https://doi.org/10.1007/978-1-61779-867-2_3

Breitling, R., Y. Li, B. M. Tesson, J. Fu, C. Wu *et al.*, 2008 Genetical genomics: spotlight on QTL hotspots. PLoS Genet. 4: e1000232. https://doi.org/10.1371/journal.pgen.1000232

Brem, R. B., and L. Kruglyak, 2005 The landscape of genetic complexity across 5,700 gene expression traits in yeast. Proc. Natl. Acad. Sci. USA 102: 1572–1577. https://doi.org/10.1073/pnas.0408709102

Broman, K. W., H. Wu, S. Sen, and G. A. Churchill, 2003 R/qtl: QTL mapping in experimental crosses. Bioinformatics 19: 889–890. https://doi.org/10.1093/bioinformatics/btg112

Bubier, J. A., J. J. Jay, C. L. Baker, S. E. Bergeson, H. Ohno *et al.*, 2014 Identification of a QTL in Mus musculus for alcohol preference, withdrawal, and Ap3m2 expression using integrative functional genomics and precision genetics. Genetics 197: 1377–1393. https://doi.org/10.1534/genetics.114.166165

Clifford, D. C., and P. McCullagh 2006 The regress function. R News 6: 6–10.

Clifford, D. C., and P. McCullagh 2014 regress: Gaussian linear models with linear covariance structure. The regress package R package version 1.3-15.

Cook, D. E., and E. C. Andersen, 2017 VCF-kit: assorted utilities for the variant call format. Bioinformatics 33: 1581–1582. https://doi.org/10.1093/bioinformatics/btx011

Cook, D. E., S. Zdraljevic, R. E. Tanny, B. Seo, D. D. Riccardi *et al.*, 2016 The genetic basis of natural variation in Caenorhabditis elegans telomere length. Genetics 204: 371–383. https://doi.org/10.1534/genetics.116.191148

Cook, D. E., S. Zdraljevic, J. P. Roberts, and E. C. Andersen, 2017 CeNDR, the Caenorhabditis elegans natural diversity resource. Nucleic Acids Res. 45: D650–D657. https://doi.org/10.1093/nar/gkw893

Cowley, Jr., A. W.., 2006 The genetic dissection of essential hypertension. Nat. Rev. Genet. 7: 829–840. https://doi.org/10.1038/nrg1967

Crusio, W. E., E. Dhawan, E. J. Chesler, and A. Delprato, 2016 Analysis of morphine responses in mice reveals a QTL on chromosome 7. F1000 Res. 5: 2156. https://doi.org/10.12688/f1000research.9484.2

Dittrich-Reed, D. R., and B. M. Fitzpatrick, 2013 Transgressive hybrids as hopeful monsters. Evol. Biol. 40: 310–315. https://doi.org/10.1007/s11692-012-9209-0

Doroszuk, A., L. B. Snoek, E. Fradin, J. Riksen, and J. Kammenga, 2009 A genome-wide library of CB4856/N2 introgression lines of Caenorhabditis elegans. Nucleic Acids Res. 37: e110. https://doi.org/10.1093/nar/gkp528

Easton, D. F., D. T. Bishop, D. Ford, and G. P. Crockford, 1993 Genetic linkage analysis in familial breast and ovarian cancer: results from 214 families. The breast cancer linkage Consortium. Am. J. Hum. Genet. 52: 678–701.

Ehrenreich, I. M., 2017 Epistasis: searching for interacting genetic variants using crosses. G3 (Bethesda) 7: 1619–1622. https://doi.org/10.1534/g3.117.042770

Ehrenreich, I. M., J. Bloom, N. Torabi, X. Wang, Y. Jia *et al.*, 2012 Genetic architecture of highly complex chemical resistance traits across four yeast strains. PLoS Genet. 8: e1002570. https://doi.org/10.1371/journal.pgen.1002570

Evans, K. S., Y. Zhao, S. C. Brady, L. Long, P. T. McGrath *et al.*, 2017 Correlations of genotype with climate parameters suggest Caenorhabditis elegans niche adaptations. G3 (Bethesda) 7: 289–298. https://doi.org/10.1534/g3.116.035162

García-González, A. P., A. D. Ritter, S. Shrestha, E. C. Andersen, L. S. Yilmaz *et al.*, 2017 Bacterial metabolism affects the C. elegans response to cancer chemotherapeutics. Cell 169: 431–441. e8. https://doi.org/10.1016/j.cell.2017.03.046

Glater, E. E., M. V. Rockman, and C. I. Bargmann, 2014 Multigenic natural variation underlies Caenorhabditis elegans olfactory preference for the bacterial pathogen Serratia marcescens. G3 (Bethesda) 4: 265–276. https://doi.org/10.1534/g3.113.008649

Gutteling, E. W., A. Doroszuk, J. A. G. Riksen, Z. Prokop, J. Reszka *et al.*, 2007a Environmental influence on the genetic correlations between life-history traits in Caenorhabditis elegans. Heredity 98: 206–213. https://doi.org/10.1038/sj.hdy.6800929

Gutteling, E. W., J. A. G. Riksen, J. Bakker, and J. E. Kammenga, 2007b Mapping phenotypic plasticity and genotype-environment interactions affecting life-history traits in Caenorhabditis elegans. Heredity 98: 28–37. https://doi.org/10.1038/sj.hdy.6800894

Hasin-Brumshtein, Y., A. H. Khan, F. Hormozdiari, C. Pan, B. W. Parks *et al.*, 2016 Hypothalamic transcriptomes of 99 mouse strains reveal trans eQTL hotspots, splicing QTLs and novel non-coding genes. Elife 5: e15614. https://doi.org/10.7554/eLife.15614

Highfill, C. A., J. H. Tran, S. K. T. Nguyen, T. R. Moldenhauer, X. Wang *et al.*, 2017 Naturally segregating variation at Ugt86Dd contributes to nicotine resistance in Drosophila melanogaster. Genetics 207: 311–325. https://doi.org/10.1534/genetics.117.300058

Hill, W. G., M. E. Goddard, and P. M. Visscher, 2008 Data and theory point to mainly additive genetic variance for complex traits. PLoS Genet. 4: e1000008. https://doi.org/10.1371/journal.pgen.1000008

Johnsson, M., K. B. Jonsson, L. Andersson, P. Jensen, and D. Wright, 2015 Quantitative trait locus and genetical genomics analysis identifies putatively causal genes for fecundity and brooding in the chicken. G3 (Bethesda) 6: 311–319. https://doi.org/10.1534/g3.115.024299

Kammenga, J. E., A. Doroszuk, J. A. G. Riksen, E. Hazendonk, L. Spiridon *et al.*, 2007 A Caenorhabditis elegans wild type defies the temperature-size rule owing to a single nucleotide polymorphism in Tra-3. PLoS Genet. 3: e34. https://doi.org/10.1371/journal.pgen.0030034

Keurentjes, J. J. B., J. Fu, I. R. Terpstra, J. M. Garcia, G. van den Ackerveken *et al.*, 2007 Regulatory network construction in Arabidopsis by using genome-wide gene expression quantitative trait loci. Proc. Natl. Acad. Sci. USA 104: 1708–1713. https://doi.org/10.1073/pnas.0610429104

Knoch, D., D. Riewe, R. C. Meyer, A. Boudichevskaia, R. Schmidt *et al.*, 2017 Genetic dissection of metabolite variation in Arabidopsis seeds: evidence for mQTL hotspots and a master regulatory locus of seed metabolism. J. Exp. Bot. 68: 1655–1667. https://doi.org/10.1093/jxb/erx049

Lachowiec, J., X. Shen, C. Queitsch, and Ö. Carlborg, 2015 A genome-wide association analysis reveals epistatic cancellation of additive genetic variance for root length in Arabidopsis thaliana. PLoS Genet. 11: e1005541. https://doi.org/10.1371/journal.pgen.1005541

Laricchia, K. M., S. Zdraljevic, D. E. Cook, and E. C. Andersen, 2017 Natural variation in the distribution and abundance of transposable elements across the Caenorhabditis elegans species. Mol. Biol. Evol. 34: 2187–2202. https://doi.org/10.1093/molbev/msx155

Leal-Bertioli, S. C. M., M. C. Moretzsohn, P. A. Roberts, C. Ballén-Taborda, T. C. O. Borba *et al.*, 2015 Genetic mapping of resistance to Meloidogyne arenaria in Arachis stenosperma: a new source of nematode resistance for peanut. G3 (Bethesda) 6: 377–390. https://doi.org/10.1534/g3.115.023044

Lee, D., H. Yang, J. Kim, S. Brady, S. Zdraljevic *et al.*, 2017 The genetic basis of natural variation in a phoretic behavior. Nat. Commun. 8: 273. https://doi.org/10.1038/s41467-017-00386-x

Li, Y., O. A. Alvarez, E. W. Gutteling, M. Tijsterman, J. Fu *et al.*, 2006 Mapping determinants of gene expression plasticity by genetical genomics in C. elegans. PLoS Genet. 2: e222. https://doi.org/10.1371/journal.pgen.0020222

Mackay, T. F., 2001 Quantitative trait loci in Drosophila. Nat. Rev. Genet. 2: 11–20. https://doi.org/10.1038/35047544

Mackay, T. F., 2015 Epistasis for quantitative traits in Drosophila. Methods Mol. Biol. 1253: 47–70. https://doi.org/10.1007/978-1-4939-2155-3_4

Mäki-Tanila, A., and W. G. Hill, 2014 Influence of gene interaction on complex trait variation with multilocus models. Genetics 198: 355–367. https://doi.org/10.1534/genetics.114.165282

Malmberg, R. L., S. Held, A. Waits, and R. Mauricio, 2005 Epistasis for fitness-related quantitative traits in Arabidopsis thaliana grown in the field and in the greenhouse. Genetics 171: 2013–2027. https://doi.org/10.1534/genetics.105.046078

Mardis, E. R., 2017 DNA sequencing technologies: 2006–2016. Nat. Protoc. 12: 213–218. https://doi.org/10.1038/nprot.2016.182

Marriage, T. N., E. G. King, A. D. Long, and S. J. Macdonald, 2014 Fine-mapping nicotine resistance loci in Drosophila using a multiparent advanced generation inter-cross population. Genetics 198: 45–57. https://doi.org/10.1534/genetics.114.162107

McGrath, P. T., M. V. Rockman, M. Zimmer, H. Jang, E. Z. Macosko *et al.*, 2009 Quantitative mapping of a digenic behavioral trait implicates globin variation in C. elegans sensory behaviors. Neuron 61: 692–699. https://doi.org/10.1016/j.neuron.2009.02.012

Najarro, M. A., J. L. Hackett, B. R. Smith, C. A. Highfill, E. G. King *et al.*, 2015 Identifying loci contributing to natural variation in xenobiotic resistance in Drosophila. PLoS Genet. 11: e1005663 [corrigenda: PLoS Genet. 12: e1005830 (2016)]. https://doi.org/10.1371/journal.pgen.1005663

Nelson, R. M., M. E. Pettersson, and Ö. Carlborg, 2013 A century after Fisher: time for a new paradigm in quantitative genetics. Trends in Genetics: TIG 29: 669–676. https://doi.org/10.1016/j.tig.2013.09.006

Peng, W., J. Xu, Y. Zhang, J. Feng, C. Dong *et al.*, 2016 An ultra-high density linkage map and QTL mapping for sex and growth-related traits of common carp (Cyprinus carpio). Sci. Rep. 6: 26693 (erratum: Sci. Rep. 6: 30101). https://doi.org/10.1038/srep26693

Pommier, Y., 2006 Topoisomerase I inhibitors: camptothecins and beyond. Nat. Rev. Cancer 6: 789–802. https://doi.org/10.1038/nrc1977

Price, N. P. J., and B. Tsvetanova, 2007 Biosynthesis of the tunicamycins: a review. J. Antibiot. (Tokyo) 60: 485–491. https://doi.org/10.1038/ja.2007.62

R Core Team, 2017 R: A Language and Environment for Statistical Computing. R Foundation for Statistical Computing, Vienna, Austria.

Reddy, K. C., E. C. Andersen, L. Kruglyak, and D. H. Kim, 2009 A polymorphism in Npr-1 is a behavioral determinant of pathogen susceptibility in C. elegans. Science 323: 382–384. https://doi.org/10.1126/science.1166527

Rockman, M. V., 2012 The QTN program and the alleles that matter for evolution: all that's gold does not glitter. Evolution 66: 1–17. https://doi.org/10.1111/j.1558-5646.2011.01486.x

Rockman, M. V., and L. Kruglyak, 2009 Recombinational landscape and population genomics of Caenorhabditis elegans. PLoS Genet. 5: e1000419. https://doi.org/10.1371/journal.pgen.1000419

Rockman, M. V., S. S. Skrovanek, and L. Kruglyak, 2010 Selection at linked sites shapes heritable phenotypic variation in C. elegans. Science 330: 372–376. https://doi.org/10.1126/science.1194208

Rodriguez, M., L. B. Snoek, J. A. G. Riksen, R. P. Bevers, and J. E. Kammenga, 2012 Genetic variation for stress-response hormesis in C. elegans lifespan. Exp. Gerontol. 47: 581–587. https://doi.org/10.1016/j.exger.2012.05.005

Rothschild, M. F., Z.-L. Hu, and Z. Jiang, 2007 Advances in QTL mapping in pigs. Int. J. Biol. Sci. 3: 192–197. https://doi.org/10.7150/ijbs.3.192

Schmid, T., L. B. Snoek, E. Fröhli, M. L. van der Bent, J. Kammenga *et al.*, 2015 Systemic regulation of RAS/MAPK signaling by the serotonin metabolite 5-HIAA. PLoS Genet. 11: e1005236. https://doi.org/10.1371/journal.pgen.1005236

Seidel, H. S., M. V. Rockman, and L. Kruglyak, 2008 Widespread genetic incompatibility in C. elegans maintained by balancing selection. Science 319: 589–594. https://doi.org/10.1126/science.1151107

Seidel, H. S., M. Ailion, J. Li, A. van Oudenaarden, M. V. Rockman *et al.*, 2011 A novel sperm-delivered toxin causes late-stage embryo lethality and transmission ratio distortion in C. elegans. PLoS Biol. 9: e1001115. https://doi.org/10.1371/journal.pbio.1001115

Shang, L., L. Ma, Y. Wang, Y. Su, X. Wang *et al.*, 2016 Main effect QTL with dominance determines heterosis for dynamic plant height in upland cotton. G3 (Bethesda) 6: 3373–3379. https://doi.org/10.1534/g3.116.034355

Shimko, T. C., and E. C. Andersen, 2014 COPASutils: an R package for reading, processing, and visualizing data from COPAS large-particle flow cytometers. PLoS One 9: e111090. https://doi.org/10.1371/journal.pone.0111090

Simon, M., O. Loudet, S. Durand, A. Bérard, D. Brunel *et al.*, 2008 Quantitative trait loci mapping in five new large recombinant inbred line populations of Arabidopsis thaliana genotyped with consensus single-nucleotide polymorphism markers. Genetics 178: 2253–2264. https://doi.org/10.1534/genetics.107.083899

Singh, K. D., B. Roschitzki, L. B. Snoek, J. Grossmann, X. Zheng *et al.*, 2016 Natural genetic variation influences protein abundances in C. elegans developmental signalling pathways. PLoS One 11: e0149418. https://doi.org/10.1371/journal.pone.0149418

Singh, U. M., S. Yadav, S. Dixit, P. J. Ramayya, M. N. Devi *et al.*, 2017 QTL hotspots for early vigor and related traits under dry direct-seeded system in rice (Oryza Sativa L.). Front. Plant Sci. 8: 286. https://doi.org/10.3389/fpls.2017.00286

Snoek, L. B., H. E. Orbidans, J. J. Stastna, A. Aartse, M. Rodriguez *et al.*, 2014 Widespread genomic incompatibilities in

Caenorhabditis elegans. G3 (Bethesda) 4: 1813–1823. https://doi.org/10.1534/g3.114.013151

Viñuela, A., L. B. Snoek, J. A. G. Riksen, and J. E. Kammenga, 2010 Genome-wide gene expression regulation as a function of genotype and age in C. elegans. Genome Res. 20: 929–937. https://doi.org/10.1101/gr.102160.109

Yang, J., B. Benyamin, B. P. McEvoy, S. Gordon, A. K. Henders *et al.*, 2010 Common SNPs explain a large proportion of the heritability for human height. Nat. Genet. 42: 565–569. https://doi.org/10.1038/ng.608

Zamanian, M., D. E. Cook, S. Zdraljevic, S. C. Brady, D. Lee *et al.*, 2018 Discovery of genomic intervals that underlie nematode responses to benzimidazoles. PLoS Negl. Trop. Dis. 12: e0006368. https://doi.org/10.1371/journal.pntd.0006368

Zdraljevic, S., and E. C. Andersen, 2017 Natural diversity facilitates the discovery of conserved chemotherapeutic response mechanisms. Curr. Opin. Genet. Dev. 47: 41–47. https://doi.org/10.1016/j.gde.2017.08.002

Zdraljevic, S., C. Strand, H. S. Seidel, D. E. Cook, J. G. Doench *et al.*, 2017 Natural variation in a single amino acid substitution underlies physiological responses to topoisomerase II poisons. PLoS Genet. 13: e1006891. https://doi.org/10.1371/journal.pgen.1006891

Zuk, O., E. Hechter, S. R. Sunyaev, and E. S. Lander, 2012 The mystery of missing heritability: genetic interactions create phantom heritability. Proc. Natl. Acad. Sci. USA 109: 1193–1198. https://doi.org/10.1073/pnas.1119675109

Communicating editor: E. Chesler